On the Statistics of Coherence Estimators for Textured Clutter Plus Noise

Christoph H. Gierull, *Senior Member, IEEE*

***Abstract*— This letter presents a theoretical analysis of the impact of thermal noise on the statistics of the classical as well as a modified estimator for the cross-correlation coefficient between two receive channels, which follow a noisy compound clutter model. This correlation coefficient, in the synthetic aperture radar (SAR) context often called coherence, is widely used as an important quality parameter in the field of SAR interferometry, SAR change detection, and SAR ground moving target indication. Based on a novel closed-form expressions for the probability density function (pdf) for integer number of averaged samples (or looks), it is shown that, contrary to widespread belief, the clutter texture does not cancel out when the noise contribution is taken into account. It is further demonstrated that the new pdfs can be used to derive the bias and variance of the sample coherence in analytical closed form. Thereby, the impact of the texture on the estimators is analyzed.**

***Index Terms*— Correlation coefficient, SAR change detection, SAR interferometry, spaceborne (SAR), synthetic aperture radar (SAR).**

I. Introduction

AFTER range and azimuth compression, the kth sample of the measured complex synthetic aperture radar (SAR) image data $Z(k)$ can be modeled as a superposition of clutter C and thermal noise N

$$Z(k) = C(k) + N(k) \in \mathbb{C}. \tag{1}$$

In the following, capital letters denote random variables and small letters denote the corresponding realizations. Transposition of a matrix is denoted by superscript $'$ and conjugate complex transpose by *, respectively. As a result of the central limit theorem, i.e., a large number of independent identically distributed scatterers in one resolution cell, the contributions C_k and N_k are modeled as realizations of identical independent complex zero-mean Gaussian random variables with variances σ_c^2 and σ_n^2, respectively. Coherently summed, they possess a Rayleigh-amplitude, which causes the "salt-and-pepper" graininess or speckle.

On the ocean, high-resolution SAR starts to resolve features caused by the roughness of the sea surface. This is mainly driven by two kinds of wave structures, namely capillary waves and gravity waves or swells. The first is typically local in nature with the velocity of propagation controlled by surface tension. Capillary waves show short wavelengths, in the order of centimeters, generated by turbulent gusts near the sea surface. In contrast, the velocity of propagation of gravity waves is controlled by gravity and generated by stable winds that blow for a sufficient time over a sufficient distance. This two-scale nature lends itself to the two-component, compound representation of the sea backscatter originally proposed by Ward [1]. Small patches of the sea surfaces, including a number of resolution cells, might still correctly be represented by a complex normal distribution with a mean capitalize Radar Cross Section value σ_c. The variation of the local power between multilook cells caused by macroscale sea features (including whitecap scattering, varying local wind structures, varying sea current conditions, or surface self-shadowing) is called the texture. The texture is generally represented through a nonnegative real random variable $\Delta \in [0, \infty)$. As the local power now changes spatially, the assembly of all image pixels will follow a non-Gaussian distribution. This distribution is typically characterized by a prolonged tail, indicating the existence of a higher probability of stronger backscatterers.

The extended model for heterogeneous clutter reads

$$Z_k = \Delta \cdot C(k) + N(k), \quad k = 1, \ldots, n \tag{2}$$

where the number of independent samples is commonly called the number of looks in the SAR literature. A widely used model for the texture random variable of sea surfaces is the square root of the Gamma-distribution [2] (which is also sometimes called Nakagami-distribution in the literature) described by its probability density function (pdf)

$$f_\Delta(\delta) = \frac{2\nu^\nu}{\Gamma(\nu)} \delta^{(2\nu-1)} \exp(-\nu\delta^2). \tag{3}$$

The texture parameter ν represents the degree of heterogeneity. It has been shown previously that when the noise is omitted, the sum of the squared magnitudes, $\sum_{k=1}^n |Z(k)|^2$, follows the classical K-distribution [2]. A chosen property of the texture model in (3) is the unity of its second moment, $\mathsf{E}\,\Delta^2 = 1$, so that the total clutter power σ_c^2 is unchanged. This constraint eliminates the second parameter typically associated with the Gamma-distribution.

Recently, it has been suggested to employ a discrete texture model represented by its pdf

$$f_\Delta(\delta) = \sum_{i=1}^{I} c_i \mathfrak{d}(\delta - a_i), \quad \sum_{i=1}^{I} c_i = 1, \; c_i \geq 0 \tag{4}$$

in which $\mathfrak{d}(\cdot)$ denotes the delta-function, $\boldsymbol{a} = [a_1, \ldots, a_I]$ are discrete texture intensity levels, and $\boldsymbol{c} = [c_1, \ldots, c_I]$ are the corresponding relative weights [3]. A physical motivation is that the clutter consists of a finite, and in most cases, rather

Manuscript received December 16, 2016; revised February 2, 2017; accepted February 12, 2017. Date of publication March 14, 2017; date of current version April 20, 2017.

The author is with Defence Research and Development Canada, Ottawa, ON, K1A 0Z4, Canada.

Color versions of one or more of the figures in this letter are available online at http://ieeexplore.ieee.org.

Digital Object Identifier 10.1109/LGRS.2017.2671747

small number I of types of scatterer that are disjoined and distinct from one another. The number I of scatterer classes to be considered for a sea clutter patch is obviously not *a priori* known, but it has been established that $I = 3$ is sufficient for virtually all practical cases [4]. Therefore, the technique has been named the trimodal discrete (3MD) sea clutter model.

In contrast to the sea surface, for many land applications, it has been shown that an inverse Gamma-distribution for the texture, i.e., $\Delta \sim \Gamma(\nu)^{-1}$, leads to favorable results due to the even more pronounced tail [5], [6].

II. Classical Sample Cross-Correlation Coefficient

Let us consider a two-channel radar, for instance, employed in SAR interferometric applications or in SAR ground moving target indication (GMTI) systems. In homogeneous terrain with $\Delta = 1$, the random variables describing one image pixel of the two channels may be denoted as Z_1 and Z_2. When concatenated into the 2-D vector $\boldsymbol{Z} = [Z_1, Z_2]'$, and assuming that

$$\boldsymbol{C} \sim \mathcal{N}_2^{\mathbb{C}}\left(\boldsymbol{0}, \sigma_c^2 \begin{bmatrix} 1 & \rho_c \\ \rho_c^* & 1 \end{bmatrix}\right) \quad \text{and } \boldsymbol{N} \sim \mathcal{N}_2^{\mathbb{C}}\left(\boldsymbol{0}, \sigma_n^2 \mathbf{I}_2\right)$$

where $\mathbf{I}_\mu$ denotes the identity matrix of size $\mu \times \mu$, leads to the bivariate Gaussian distribution for $\boldsymbol{Z}$ with correlation coefficient $\mathsf{E}\, Z_1 Z_2^* = \rho = \sigma_c^2 \rho_c / (\sigma_c^2 \rho_c + \sigma_n^2)$. Note that vectors are written in bold. The classical maximum-likelihood estimator for the cross-correlation coefficient reads

$$T = \frac{\left|\sum_{k=1}^n Z_1(k) Z_2(k)^*\right|}{\sqrt{\sum_{k=1}^n |Z_1(k)|^2} \sqrt{\sum_{k=1}^n |Z_2(k)|^2}} \tag{5}$$

such that $0 \le T \le 1$. The distribution of T has originally been derived by Goodman [7], see also [8]. Its pdf is given by

$$f_T(t) = 2(n-1)(1-|\rho|^2)^n t (1-t^2)^{n-2} {}_2\mathrm{F}_1(n, n; 1; |\rho|^2 t^2) \tag{6}$$

in which ${}_2\mathrm{F}_1(\cdot)$ represents Gauss' hypergeometric function. In the paper by Touzi *et al.* [9], it has been shown that the mean value can be described by a higher order hypergeometric function, ${}_3F_2(\cdot)$. Through numerical analysis, it was demonstrated that the estimator T is always biased, particularly for small correlation values. This is understandable, since the pdf is always positive one-sided, which means that for $\rho = 0$, the pdf must be a delta-function in order to create unbiased estimates.

It is easy to see that for the simplified models, i.e., omitted noise with $\boldsymbol{Z} = \Delta \boldsymbol{C}$ or textured noise $\boldsymbol{Z} = \Delta(\boldsymbol{C} + \boldsymbol{N})$, that the pdf (6) remains unchanged, because the texture in (5) cancels out provided Δ is assumed identical for both channels and stays constant over the sample set $k = 1, \ldots, n$. As discussed in several papers, these models, however, are of limited practical utility, especially for space-based SAR.

Using instead the general model $\boldsymbol{Z} = \Delta \boldsymbol{C} + \boldsymbol{N}$, and keeping the texture random variable fixed, i.e., $\Delta = \delta$, yield for the conditional random vector $\boldsymbol{Z}|\Delta := (\boldsymbol{Z}|\Delta = \delta)$ again a multivariate complex normal distribution

$$\boldsymbol{Z}|\Delta \sim \mathcal{N}_2^{\mathbb{C}}\left(\boldsymbol{0}, (\delta^2 \sigma_c^2 + \sigma_n^2) \begin{bmatrix} 1 & \rho(\delta) \\ \rho(\delta)^* & 1 \end{bmatrix}\right). \tag{7}$$

The magnitude of the correlation coefficient in (7) is

$$\rho_\delta := |\rho(\delta)| = \left|\frac{\delta^2 \rho_c \sigma_c^2 / \sigma_n^2}{\delta^2 \rho_c \sigma_c^2 / \sigma_n^2 + 1}\right| \tag{8}$$

and now depends on the texture as well as the Clutter-to-Noise Ratio (CNR). According to (5), the conditional correlation coefficient has the pdf

$$f_{T|\Delta}(t) = 2(n-1)(1-\rho_\delta^2)^n t (1-t^2)^{n-2} \left(n, n; 1; \rho_\delta^2 t^2\right). \tag{9}$$

For integer number of looks, [8] provides an alternative closed-form expression for (6) involving an infinite summation. In Appendix IV, it is shown that it is possible to find a novel analytical expression including only a finite sum, namely

$$f_{T|\Delta}(t) = 2(n-1)(1-\rho_\delta^2)^n \frac{t(1-t^2)^{n-2}}{\left(1-\rho_\delta^2 t^2\right)^{2n-1}} \times \sum_{k=0}^{n-1} \binom{n-1}{k}^2 (\rho_\delta t)^{2(n-k-1)}, \quad 0 \le \rho_\delta < 1 \tag{10}$$

where $\binom{\cdot}{\cdot}$ denotes the binomial coefficient. This expression allows to compute central moments or the cdf more efficiently and accurately especially for large n and arguments close to the unit circle. Integrating the conditional pdf with respect to the texture pdf yields the marginal pdf

$$f_T(t) = \int_0^\infty f_{T|\Delta}(t, \delta) f_\Delta(\delta) d\delta. \tag{11}$$

For the texture model (4), the pdf yields the closed form

$$f_T(t) = 2(n-1)(1-t^2)^{n-2} \sum_{k=0}^{n-1} \binom{n-1}{k}^2 t^{2(n-k)-1} \times \sum_{i=0}^{I} c_i \frac{\left(1-\rho_{a_i}^2\right)^n \rho_{a_i}^{2(n-k-1)}}{\left(1-\rho_{a_i}^2 t^2\right)^{2n-1}} \tag{12}$$

where ρ_{a_i} is given in (8) when δ is replaced by a_i. For the Nakagami-distribution (3), the pdf can numerically be evaluated. In fact, this is true for any other texture model for which a pdf $f_\Delta(\delta)$ exists.

Fig. 1 shows the impact of the noise on the pdf of the sample coherence for fully correlated clutter $\rho_c = 1$, and a CNR = 7 dB. The texture parameters in (12) have been arbitrarily chosen to be $\boldsymbol{c} = [0.065, 0.608, 0.326]$ and $\boldsymbol{a} = [1.486, 1.133, 0.483]$ representing heterogeneous clutter [4]. In comparison, the green curve shows the pdf (6) with $\rho = \sigma_c^2/\sigma_n^2 / (\sigma_c^2/\sigma_n^2 + 1) = 0.8337$. It can be seen that pdf shifts its center of gravity to the left thereby likely increasing the bias toward smaller values. Fig. 2 shows the same effect for the Gamma texture model for a somewhat smaller CNR = 3 dB and a texture parameter $\nu = 5$, again representing rather heterogeneous background.

In contrast to the simulations in [10] or the numerical solutions used in [9], (10) can be exploited to find analytical closed-form solutions for the mean and variance albeit becoming somewhat cumbersome for larger values of n. As an example, using the result in Appendix IV, the mean, for $n = 4$

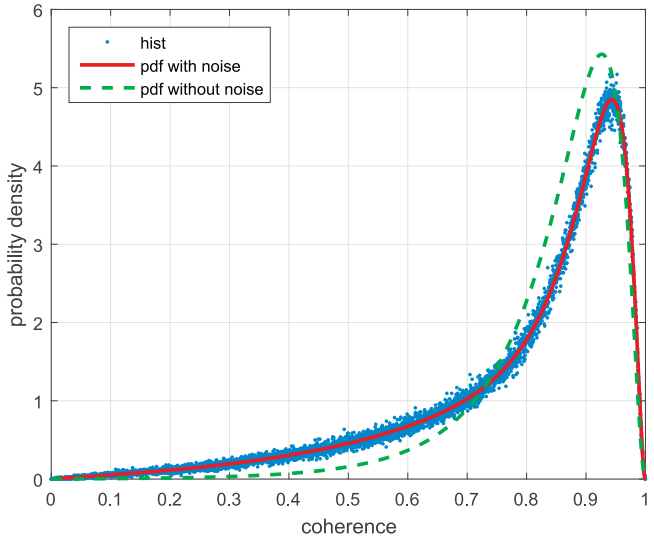

Fig. 1. PDF of sample coherence for the 3MD texture model.

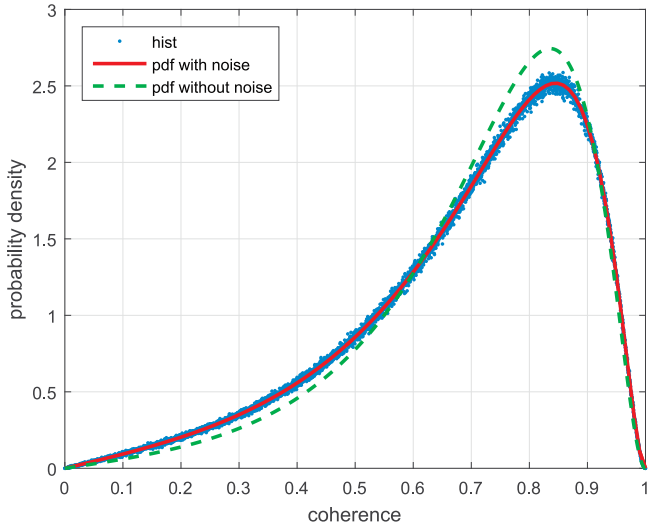

Fig. 2. PDF of sample coherence for the Gamma texture model.

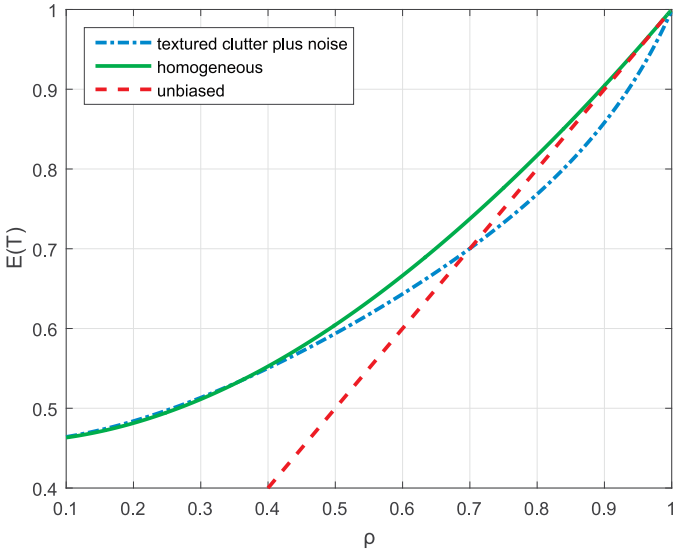

Fig. 3. Bias of the sample coherence for textured clutter plus noise.

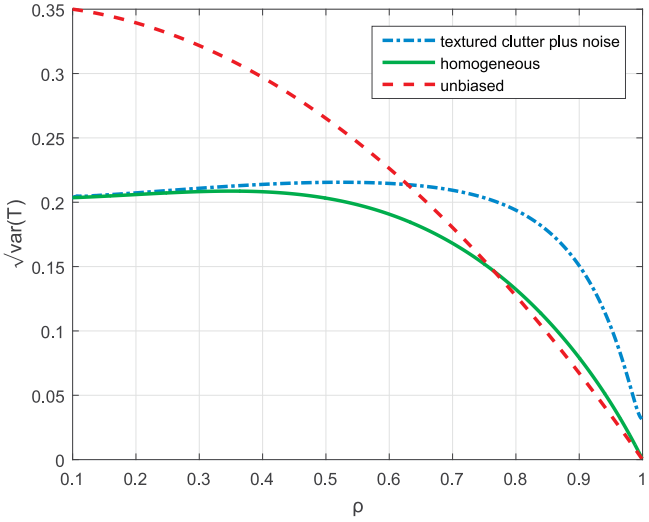

Fig. 4. Cramer Rao Bound of the sample coherence for textured clutter plus noise.

and $\rho_\delta > 0$, reads

$$\begin{aligned}\mathsf{E}(T|\Delta) = {} & \frac{75}{128}\rho_\delta^{-7}\mathrm{a}_\delta - \frac{75}{128}\rho_\delta^{-6} - \frac{306}{128}\rho_\delta^{-5}\mathrm{a}_\delta + \frac{477}{128}\rho_\delta^{-3}\mathrm{a}_\delta \\ & - \frac{348}{128}\rho_\delta^{-1}\mathrm{a}_\delta + \frac{117}{128}\rho_\delta\mathrm{a}_\delta - \frac{18}{128}\rho_\delta^{3}\mathrm{a}_\delta + \frac{3}{128}\rho_\delta^{5}\mathrm{a}_\delta \\ & + \frac{281}{128}\rho_\delta^{-4} - \frac{390}{128}\rho_\delta^{-2} + \frac{298}{128}\rho_\delta + \frac{17}{128}\rho_\delta^{2} - \frac{3}{128}\rho_\delta^{4}\end{aligned} \tag{13}$$

where E denotes the expectation operator and $\mathrm{a}_\delta = \operatorname{arctanh}(\rho_\delta)$. Integrating (13) with respect to the pdf of Δ can be used to determine the bias for the realistic compound model when the thermal receiver noise is accounted for. Obviously, for $\delta = 1$, (13) expresses the mean of the well-known classical estimator (5) corresponding to the pdf (6).

Fig. 3 shows the bias of the sample coherence for textured clutter plus noise versus ρ (or the CNR) and $n = 4$. For the texture, the discrete clutter model was applied in which the parameters were chosen to $\boldsymbol{c} = [0.1184, 0.5406, 0.3410]$ and $\boldsymbol{a} = [0.3829, 0.8477, 1.3199]$. The sum of the squared magnitudes for these texture parameters closely resembles the K-pdf with texture parameter $\nu = 5$ and as such represent a practical case oftentimes used for user requirement specifications [11]. As expected, the bias is unchanged for low coherence as the texture does only affect the clutter and not the noise. It can be observed that the bias is increasing for larger values of ρ, in fact toward smaller values as was already expected from the shape of the pdf in Fig. 1. The bias then disappears again when the CNR approaches infinity, i.e., $\rho = 1$, when the texture random variable cancels out.

The second moment for $n = 4$ and $\rho_\delta > 0$ becomes

$$\begin{aligned}\mathsf{E}(T|\Delta)^2 = {} & 3\mathrm{lg}_\delta\rho_\delta^{-8} - 12\rho_\delta^{-6}\mathrm{lg}_\delta + 18\rho_\delta^{-4}\mathrm{lg}_\delta - 12\rho_\delta^{-2}\mathrm{lg}_\delta \\ & + 3\mathrm{lg}_\delta + 3\rho_\delta^{-6} - \frac{21}{2}\rho_\delta^{-4} + 13\rho_\delta^{-2} - \frac{13}{2}\end{aligned} \tag{14}$$

with $\mathrm{lg}_\delta = \log(1 - \rho_\delta^2)$.

Fig. 4 shows the standard deviation (std) of the sample coherence for both the cases, homogeneous, nontextured clutter and the compound model, clearly demonstrating that the variance may increase considerably for larger values of correlations. This is quite counterintuitive and not expected.

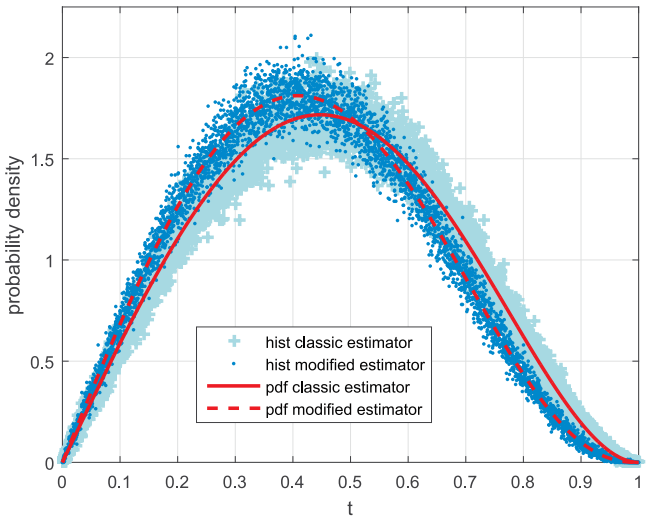

Fig. 5. Histogram and theoretical pdf of the modified interlook cross-correlation coefficient compared with the classical one.

The red curve represents the asymptotic Cramer–Rao Bound for any unbiased estimator derived in [9].

III. Modified Sample Cross-Correlation Coefficient

Recently, a variant of the sample correlation coefficient has been proposed in the literature [12]. Here, the denominator contains the average of the sample variants rather than the product of their square roots, assuming that the underlying variances are identical

$$\bar{T} = \frac{2\sum_{k=1}^{n} Z_1(k)Z_2(k)^*}{\sum_{k=1}^{n}|Z_1(k)|^2 + \sum_{k=1}^{n}|Z_2(k)|^2} := Se^{j\phi}. \quad (15)$$

The bivariate density function between the magnitude S and phase ϕ in (15) has been derived in [13]

$$f_{S,\phi}(s,\varphi) = \pi^{-1}\left(n-\frac{1}{2}\right)(1-\rho^2)^n \frac{s(1-s^2)^{n-\frac{3}{2}}}{(1-\rho s\cos\varphi)^{2n}} \quad (16)$$

for $0 \le s \le 1$ and $-\pi \le \varphi \le \pi$. Note that S and ϕ are not statistically independent. Furthermore, in contrast to T in (5), S is also valid for single-look data, i.e., for $n = 1$. The marginal density of S may be calculated via integration

$$f_S(s) = \int_{-\pi}^{\pi} f_{S,\phi}(s,\varphi)d\varphi = 2\int_{0}^{\pi} f_{S,\phi}(s,\varphi)d\varphi. \quad (17)$$

Inserting (16) into (17) and using [14, eq. (3.661-4)] yields

$$f_S(s) = 2(n-\frac{1}{2})\frac{(1-\rho^2)^n}{(1-\rho^2 s^2)^n} s(1-s^2)^{n-\frac{3}{2}} \times P_{2n-1}\left(\frac{1}{\sqrt{(1-\rho^2 s^2)}}\right) \quad 0 \le \rho < 1 \quad (18)$$

where $P(\cdot)$ denotes the Legrendre function of the first kind, which for integer n can be expressed as the finite sum

$$P_{2n-1}(x) = 2^{2n-1}\sum_{k=0}^{2n-1}\binom{2n-1}{k}\binom{(2(n-1)+k)/2}{n}x^k \quad (19)$$

so that

$$f_S(s) = 2\left(n-\frac{1}{2}\right)\left(\frac{1-\rho^2}{1-\rho^2 s^2}\right)^n \times \sum_{k=0}^{2n-1}\binom{2n-1}{k}\binom{(2(n-1)+k)/2}{n}\frac{s(1-s^2)^{n-\frac{3}{2}}}{(1-\rho^2 s^2)^{\frac{k}{2}}}. \quad (20)$$

As before, replacing ρ in (20) with ρ_δ and integrating with respect to δ allow us to study the impact of the texture on the modified sample coherence. As an example, Fig. 5 compares the pdfs of the magnitudes of the classical sample correlation coefficient with the modified one for $\rho_c = 0$ (or $\sigma_n^2 = 0$) in which case, the dependence on the texture vanishes. It can be seen that the modified estimator has a slightly smaller bias in this case. In fact, integrating (18) for $\rho = 0$ yields $\mathsf{E}\,S = (n-(1/2))B((3/2), n-(1/2))$ and $\mathsf{E}\,S^2 = (n-(1/2))/(n^2-(1/4))$, which are both smaller than the respective results in Appendix IV for all n. $B(\cdot,\cdot)$ denotes the beta-function.

IV. Conclusion

This letter extended the theoretical analysis of the magnitude sample cross-correlation coefficient between two SAR channels to the case of compound clutter in noise. These channels can be either physically located on top of each other as for single-path SAR interferometry or in flight direction for SAR GMTI. They can also be measurements from two different passes such as in change detection. One main contribution of this letter is the new analytical closed-form expression of the pdf for the sample coherence, which for the first time permits the derivation of the central moments in closed form. Based on these expressions, the bias and standard deviation were calculated for the realistic textured clutter plus noise SAR data model. It was demonstrated that texture in noisy SAR data has an impact that may be practically relevant in very heterogeneous clutter. Coherence maps estimated with only a few samples, as in SAR interferometry and coherent change detection, must be carefully interpreted even for areas with higher correlation. In addition, this letter presented a new closed-form pdf for a modified coherence estimator, which has recently attracted some interest.

Appendix A
Gauss' Hypergeometric Function

To find closed-form expression for the pdf in (6), we intend to reexpress the Gauss' hypergeometric function ${}_2\mathrm{F}_1(n, n; 1; x)$ for $n \in \mathbb{N}_{>0}$. A recursion formula is [14]

$${}_2\mathrm{F}_1(a+n, b+n; c; x) = \frac{\frac{\partial^n}{\partial x^n}\left[x^{b+n+1}\left\{\frac{\frac{\partial^n}{\partial x^n}(x^{a+n-1}\,{}_2\mathrm{F}_1(a,b;c;x))}{(a)_n x^{a-1}}\right\}\right]}{(b)_n x^{b-1}} \quad (21)$$

where $(\mu)_n = (\Gamma(n+\mu))/(\Gamma(\mu))$ represents the Pochhammer symbol. For $a = b = c = 1$, one gets

$${}_2\mathrm{F}_1(n+1, n+1; 1; x) = \frac{\frac{\partial^n}{\partial x^n}\left(x^n\left\{\frac{\partial^n}{\partial x^n}x^n\,{}_2\mathrm{F}_1(1,1;1;x)\right\}\right)}{\Gamma(n+1)^2}. \quad (22)$$

Using ${}_2\mathrm{F}_1(1,1;1;x) = (1-x)^{-1}$, and after some elementary algebra, it can be seen that the nth derivative of the inner expression reads

$$\frac{\partial^n}{\partial x^n}\left(\frac{x^n}{1-x}\right) = \frac{\Gamma(n+1)}{(1-x)^{n+1}} \tag{23}$$

so that (22) reduces to

$${}_2\mathrm{F}_1(n+1,n+1;1;x) = \frac{1}{\Gamma(n+1)}\frac{\partial^n}{\partial x^n}\left(\frac{x^n}{(1-x)^{n+1}}\right). \tag{24}$$

By observing that the first few derivations in (24) reduce to

$$\begin{aligned}
n=0:&\quad \frac{1}{1-x}\\
n=1:&\quad \frac{1+x}{(1-x)^3}\\
n=2:&\quad 2\frac{x^2+4x+1}{(1-x)^5}\\
n=3:&\quad 6\frac{x^3+9x^2+9x+1}{(1-x)^7}\\
n=4:&\quad 24\frac{x^4+16x^3+36x^2+16x+1}{(1-x)^9}\\
n=5:&\quad 120\frac{x^5+15x^4+100x^3+100x^2+25x+1}{(1-x)^{11}}
\end{aligned}$$

it can be quite easily deduced that

$${}_2\mathrm{F}_1(n,n;1;x) = \sum_{k=0}^{n-1}\frac{\binom{n-1}{k}^2 x^{n-k-1}}{(1-x)^{2n-1}} \tag{25}$$

resulting in (10). For $x=0$, only the term for $k=n-1$ survives so that as expected, ${}_2\mathrm{F}_1(n,n;1;0)=1$ for any n.

Appendix B
First Moments of the Classical Sample Coherence

The integration $\mathsf{E}\,T = \int_0^1 t f_T(t)dt$ for the pdf in (10) leads one to evaluate several integrals of the form

$$\int_0^1 \frac{t^{2(n-k)}(1-t^2)^{n-2}}{(1-\rho^2t^2)^{2n-1}}dt \quad \text{for } k=0,\ldots,n-1. \tag{26}$$

Unfortunately, no closed solution is known for a variable number of looks n. However, for particular values, analytical expressions are found for $0<\rho<1$ [15], e.g., $n=3$, $k=2$

$$\begin{aligned}
\int_0^1 \frac{t^2(1-t^2)}{(1-\rho^2t^2)^5}dt &= \frac{15\rho^6-55\rho^4+73\rho^2+15}{384\rho^2(\rho^2-1)}\\
&\quad -\frac{3\,\mathrm{arctanh}(\rho)}{128\rho^5}+\frac{3\rho^6-11\rho^4-11\rho^2+3}{128\rho^4(\rho^2-1)}\\
&\quad -\frac{5\,\mathrm{arctanh}(\rho)}{128\rho^3}.
\end{aligned} \tag{27}$$

Continuing this for the other combinations leads after some basic algebra to the polynomial expression

$$\mathsf{E}\,T = \sum_{k=-2(n-1)}^{2(n-1)}\alpha_n(k)\rho^{k-1}\mathrm{arctanh}(\rho)^{\mathrm{mod}(k-1,2)} \tag{28}$$

in which $\mathrm{mod}(\cdot,\cdot)$ denotes the modulo operation and the coefficients for the first few looks, for instance, read

$$\begin{aligned}
\alpha_2 &= [1,3,-2,-1,1]/2\\
\alpha_3 &= [-1,1,12,31,-30,-25,28,9,-9]/16\\
\alpha_4 &= [3,-3,-18,17,117,298,-348,-390,477,\\
&\qquad 281,-306,-75,75]/128\\
\alpha_5 &= [-75,75,456,-431,-1380,1243,6360,16489,\\
&\qquad -21810,-30023,39480,32491,-37956,-17375,\\
&\qquad 18600,3675,-3675]/6144.
\end{aligned}$$

For the special case $\rho=0$, it is easier to compute $\int_0^1 t^2(1-t^2)^{n-2}dt$, which leads to $\mathsf{E}\,T=(n-1)B((3/2),n-1)$. In the same way, the second moment can be derived via

$$\mathsf{E}\,T^2 = \sum_{k=0}^{n}(\beta_n(k)+\gamma_n(k)\log(1-\rho^2))\rho^{-2k} \tag{29}$$

where for instance

$$\begin{aligned}
\beta_2 &= [2,-1,0] \quad \gamma_2=[-1,2,-1]\\
\beta_3 &= [4,-5,2,0] \quad \gamma_3=[-2,6,-6,2]\\
\beta_4 &= [13/2,-13,21/2,-3,0] \quad \gamma_4=[-3,12,-13,12,-3].
\end{aligned}$$

The second moment for $\rho=0$ integrates to $\mathsf{E}\,T^2=1/n$.

References

[1] K. D. Ward, "Compound representation of high resolution sea clutter," *Electron. Lett.*, vol. 17, no. 16, pp. 561–563, Aug. 1981.

[2] K. D. Ward, R. J. A. Tough, and S. Watts, *Sea Clutter: Scattering, the K Distribution and Radar Performance* (Radar, Sonar & Navigation Series), vol. 20. London, U.K.: IET, 2006.

[3] C. H. Gierull and I. C. Sikaneta, "Processing synthetic aperture radar images for ship detection," U.S. Patent 2017/0016987 A1, Jan. 19, 2017.

[4] C. H. Gierull and I. C. Sikaneta, "Improved SAR vessel detection based on discrete texture," in *Proc. EUSAR*, Hamburg, Germany, 2016.

[5] I. Sikaneta and C. H. Gierull, "Two-channel SAR ground moving target indication for traffic monitoring in urban terrain," in *Proc. ISPRS Workshop CMRT*, vol. 36. Vienna, Austria, Aug. 2005, pp. 95–101.

[6] C. H. Gierull, I. Sikaneta, and D. Cerutti-Maori, "Two-step detector for RADARSAT-2's experimental GMTI mode," *IEEE Trans. Geosci. Remote Sens.*, vol. 51, no. 1, pp. 436–454, Jan. 2013.

[7] N. R. Goodman, "Statistical analysis based on a certain multivariate complex Gaussian distribution (an introduction)," *Ann. Math. Statist.*, vol. 34, no. 1, pp. 152–177, 1963.

[8] R. A. J. Tough, D. Blacknell, and S. Quegan, "A statistical description of polarimetric and interferometric synthetic aperture radar data," *Proc. Roy. Soc. London A*, vol. 449, pp. 567–589, Jun. 1995.

[9] R. Touzi, A. Lopes, J. Bruniquel, and P. W. Vachon, "Coherence estimation for SAR imagery," *IEEE Trans. Geosci. Remote Sens.*, vol. GRS-37, no. 1, pp. 135–149, Jan. 1999.

[10] A. M. Guarnieri and C. Prati, "SAR interferometry: A 'quick and dirty' coherence estimator for data browsing," *IEEE Trans. Geosci. Remote Sens.*, vol. 35, no. 3, pp. 660–669, May 1997.

[11] C. H. Gierull and I. Sikaneta, "Potential marine moving target indication (MMTI) performance of the RADARSAT constellation mission (RCM)," in *Proc. 9th Eur. Conf. Synth. Aperture Radar (EUSAR)*, 2012, pp. 404–407.

[12] D. E. Wahl, D. A. Yocky, C. V. Jakowatz, and K. M. Simonson, "A new maximum-likelihood change estimator for two-pass SAR coherent change detection," *IEEE Trans. Geosci. Remote Sens.*, vol. 54, no. 4, pp. 2460–2469, Apr. 2016.

[13] T. Berger, "On the correlation coefficient of a bivariate, equal variance, complex Gaussian sample," *Ann. Math. Statist.*, vol. 43, no. 6, pp. 2000–2003, 1972.

[14] I. S. Gradshteyn and I. M. Ryzhik, *Table of Integrals, Series, and Products*, A. Jeffrey and D. Zwillinger, Eds., 6th ed. New York, NY, USA: Academic, 2000.

[15] MathWorks. *Symbolic Math Toolbox*, accessed on Mar. 1, 2016. [Online]. Available: https://www.mathworks.com/products/symbolic/